

Multi-photon regime of non-linear Breit-Wheeler and Compton processes in short linearly and circularly polarized laser pulses

A. I. Titov*

Bogoliubov Laboratory of Theoretical Physics, JINR, Dubna 141980, Russia

A. Otto, and B. Kämpfer

*Helmholtz-Zentrum Dresden-Rossendorf, 01314 Dresden, Germany,
Institut für Theoretische Physik, TU Dresden, 01062 Dresden, Germany*

Non-linear Breit-Wheeler e^+e^- pair production and its crossing channel - the non-linear Compton process - in the multi-photon regime are analyzed for linearly and circularly polarized short laser pulses. The contribution of multi-photon processes to total cross sections is determined and we also show that (i) the azimuthal angular distributions of outgoing electrons in these processes differ on a qualitative level, and (ii) they depend on the polarization properties of the pulses. A finite carrier envelope phase ϕ_{CEP} leads to a non-trivial non-monotonic behavior of the azimuthal angle distributions of the considered processes. That effect can be used for the ϕ_{CEP} determination.

PACS numbers: 12.20.Ds, 13.40.-f, 23.20.Nx

Keywords: non-linear QED, carrier envelope phase, multi-photon processes, sub-threshold energies

The non-linear Breit-Wheeler (BW) process refers to the decay of a probe photon γ' (energy ω' , four-momentum k') into an electron-positron (e^+e^-) pair while traversing a laser pulse (characterized by central frequency ω , wave four-vector k and polarization four-vector a with $a \cdot k = 0$, where the dot stands for the scalar product), symbolically $\gamma' \rightarrow e_L^- + e_L^+$. Here, the label “L” points to the laser-dressed e^\pm wave functions. The non-linear Compton (C) scattering, symbolically $e_L \rightarrow \gamma' + e_L'$, as related (by crossing symmetry on amplitude level) to the BW process, is also a subject of intensive study.

In the plane-wave approximation, one can further distinguish monochromatic laser beams with an infinitely long duration (the infinite-pulse approximation [IPA]) or a pulse of finite duration (the finite-pulse approximation [FPA]). In the latter case, the bandwidth effects cause a distribution of frequencies around the central one, as evidenced by the power spectrum of the pulse. The IPA case has been analyzed in depth by the Ritus group [1] some time ago and summarized in a well-known review paper [2]. For completeness, we mention the pioneering papers by Reiss [3] and the review papers [4–6], see also recent publications [7–10]. It turned out that the polarization of the laser has a noticeable impact on the pair-production probability due to the different angular momenta of the emerging e_L^\pm . (For a complete treatment of polarization effects, cf. [11].)

Note that the kinematics of non-linear C and BW processes are vastly different. In the weak-field regime, $\xi \ll 1$ (with ξ the reduced field intensity [12] defined in our context in Eq. (3) below) where the series expansion in powers of the fine-structure constant α applies, the physical regions over the Mandelstam $s - t - u$

plane are fairly different [12, 13]. This is related to the fact that BW is a threshold process requiring $s > 4m^2$ (where s and m are the square of the total energy in the center of mass system (c.m.s.) and the electron mass, respectively), while C has a Thomson limit and is allowed at $s > m^2$, i.e. it is always above the threshold. These differences continue into the multi-photon and non-perturbative regimes. In the case of the BW process, it is natural to use the dimensionless threshold variable $\zeta = 4m^2/s$ [14] instead of s . The region $\zeta > 1$ automatically selects the sub-threshold multi-photon regime. The SLAC experiment E-144 [15] has tested this multi-photon regime at $\xi \leq 0.35$ by the trident process $e^- + L \rightarrow e^- + e^+ + e^-$ which combines the subprocesses of non-linear Compton backscattering $e^- + L \rightarrow e^- + \gamma'$ and non-linear BW. The envisaged LUXE experiment [16] will probe the non-linear BW process at $\xi > 1$. The photons γ' are thereby delivered by bremsstrahlung of the XFEL driver-beam (L) with energies $\mathcal{O}(10 \text{ GeV})$. The LUXE laser, when less tightly focused, therefore also provides access to the multi-photon regime and can be used for benchmarking issues. Note also the interesting goal of LUXE as access to “measuring the boiling point of the vacuum of quantum electrodynamics” [17]. The search for a possible manifestation of multi-photon regime in Compton scattering in analogy with BW seems to be important and is the subject of our present work.

Since high and ultrahigh laser intensities are customarily achieved by chirped pulse amplification, one is forced to take into account the effect of the pulse duration, i.e. one has to analyze the FPA case. A number of important phenomena associated with non-linear C and BW processes within finite pulses are discussed in the above-mentioned review papers. Some further entries in the fairly extended literature are given by Refs. [18–26] and [27–35], respectively.

Below, we focus on intense optical lasers with reduced

*atitov@theor.jinr.ru

field intensity $\xi^2 \leq 0.1$ as well as short and very short laser pulses with a small or very small number of field oscillations. Considering both the total cross sections and the azimuthal angle distributions of the outgoing particles, we identify observables sensitive to the initial pulse polarization, taking into account a finite carrier envelope phase ϕ_{CEP} [36, 37]. The manifestation of the carrier envelope phase, sometimes called “the absolute phase of the laser pulse” [38], is a peculiar quantum-mechanical phenomenon. It manifests itself in many diverse processes involving laser pulses, such as the e^+e^- pair production [29], non-linear Compton scattering [39, 40], electron tunneling in a coupled double-quantum-dot system [41], and strong-field ionization [42]. In the considered C and BW processes, this phenomenon is related to a non-trivial interference of the outgoing or probe photons with the background laser field.

The aim of the present study is to give a comparative sequential analysis of two elementary quantum processes in a coherent electromagnetic (e.m.) field (i.e. laser pulses with finite pulse duration) with linear and circular polarizations in the multi-photon regime for non-asymptotic kinematics, attainable at existing laser facilities, thus highlighting the most important observables.

Our paper is organized as follows. In Sect. II we discuss the laser field model. The non-linear Breit-Wheeler process and the non-linear Compton scattering are analyzed in Sects. III and IV, respectively. Our summary is given in Sect. V. In the Appendix, for convenience and easy reference, we provide some useful expressions of the infinite-pulse approximation.

I. THE LASER FIELD MODEL

We first assume that the external electric field (laser pulse) is determined by the electromagnetic (e.m.) four-potential in the radiation gauge $A^i = (0, \mathbf{A}^i)$ as $\mathbf{E}^i = -\partial \mathbf{A}^i / \partial t$, where the label $i = 0$ or 1 corresponds to the linear (*lin*) or circular (*circ*) polarizations, respectively:

$$\mathbf{A}^{(i)}(\phi) = f(\phi) [\mathbf{a}_1 \cos(\phi + \phi_{CEP}) + \delta^{i1} \mathbf{a}_2 \sin(\phi + \phi_{CEP})], \quad (1)$$

where δ^{ij} is the Kronecker delta. Thus, $\mathbf{A}^{(0)} \equiv \mathbf{A}^{(lin)}$ and $\mathbf{A}^{(1)} \equiv \mathbf{A}^{(circ)}$. The quantity $\phi = k \cdot x$ is the invariant phase with wave four-vector $k = (\omega, \mathbf{k})$, obeying the null-field property $k^2 = k \cdot k = 0$ implying $\omega = |\mathbf{k}|$, $\mathbf{a}_{(1,2)} \equiv \mathbf{a}_{(x,y)}$; $|\mathbf{a}_x|^2 = |\mathbf{a}_y|^2 = a^2$, $\mathbf{a}_x \cdot \mathbf{a}_y = 0$; transversality means $\mathbf{k} \cdot \mathbf{a}_{x,y} = 0$ in the present gauge; in addition, $A_z = 0$. For the sake of definiteness, the envelope function $f(\phi)$ is chosen as hyperbolic secant:

$$f(\phi) = \frac{1}{\cosh \frac{\phi}{\Delta}}. \quad (2)$$

The dimensionless quantity Δ is related to the pulse duration $2\Delta = 2\pi N$, where N characterizes the number of

cycles in the pulse. It is related to the time duration of the pulse $\tau = 2N/\omega$. $N < 1$ means sub-cycle pulses (for the dependence of some observables on the envelope shape, see [30] for example).

The quantity ϕ_{CEP} is the carrier envelope phase (CEP). The interplay of CEP and the azimuthal angle of the outgoing electron is important and will be the subject of detailed considerations below.

For convenience, we recollect the relation between $\xi^2 = e^2 a^2 / m^2$ and the averaged laser pulse intensity $\langle I_L \rangle$ for circularly/linearly polarized pulses [14]

$$\xi^2 = \frac{N}{N_0^{(i)}} \frac{5.62 \cdot 10^{-19}}{\omega_{[eV^2]}^2} \langle I_L \rangle_{[\frac{W}{cm^2}]}. \quad (3)$$

The normalization factors $N_0^{(i)}$ are related to the average density of the e.m. field $\langle \mathcal{E} \rangle$ and are expressed through the envelope functions as

$$\begin{aligned} N_0^{(lin)} &= \frac{1}{2\pi} \int_{-\infty}^{\infty} d\phi \left(f^2(\phi) + f'^2(\phi) \right) \cos^2 \phi, \\ N_0^{(circ)} &= \frac{1}{2\pi} \int_{-\infty}^{\infty} d\phi \left(f^2(\phi) + f'^2(\phi) \right) \end{aligned} \quad (4)$$

with the asymptotic values at $\Delta/\pi \gg 1$: $N_0^{(circ)} \simeq \Delta/\pi$, and $N_0^{(lin)} \simeq \Delta/2\pi$.

We use natural units with $c = \hbar = 1$, $e^2/4\pi = \alpha \approx 1/137.036$.

II. NON-LINEAR BREIT-WHEELER PROCESS

A. Cross sections

As mentioned above, we consider essentially multi-photon events, where a finite number of laser photons are involved in the e^+e^- -pair production. This allows for sub-threshold e^+e^- -pair production with $s < s_{thr}$ or $\zeta > 1$. In the following, we analyze the dependence of cross sections on ζ and on the e.m. field intensity which is described by the reduced field intensity parameter ξ^2 . We will also analyze the differential cross sections as a function of the azimuthal angle of the outgoing electron (or positron) for different values ϕ_{CEP} . In all cases, we provide a direct comparison of results for linear and circular polarizations.

The differential cross sections read

$$\frac{d\sigma^{(i)}}{d\phi_e} = \frac{\alpha^2 \zeta}{4m^2 \xi^2 N_0^{(i)}} \int_{\zeta}^{\infty} d\ell v(\ell) \int_{-1}^1 d\cos\theta_e w^{(i)}(\ell), \quad (5)$$

where ℓ is here an auxiliary continuous variable. The azimuthal angle of the outgoing electron, ϕ_e , is defined as $\cos\phi_e = \mathbf{a}_x \cdot \mathbf{p}_e / a |\mathbf{p}_e|$. It is related to the azimuthal

angle of the positron by $\phi_{e^+} = \phi_e + \pi$. Furthermore, θ_e is the polar angle of the outgoing electron, v is the electron (positron) velocity in the center of mass system (c.m.s.).

The lower limit of the integral over the variable ℓ is the threshold parameter ζ . The region of $\zeta < 1$ corresponds to the above-threshold e^+e^- -pair production, while the region of $\zeta > 1$ is for the sub-threshold pair production enabled by multi-photon and bandwidth effects. We keep our notation of [31] and denote by $k(\omega, \mathbf{k})$, $k'(\omega', \mathbf{k}')$, $p(E, \mathbf{p})$ and $p'(E', \mathbf{p}')$ the four-momenta of the background (laser) field (1), the incoming probe photon, the outgoing positron and the outgoing electron, respectively. The important variables s , v and u are determined by $s = 2\mathbf{k} \cdot \mathbf{k}' = 2(\omega'\omega - \mathbf{k}'\mathbf{k})$ (with $\mathbf{k}'\mathbf{k} = -\omega'\omega$ for head-on geometry), $v^2 = (\ell s - 4m^2)/\ell s$, $u \equiv (k' \cdot k)^2 / (4(k \cdot p)(k \cdot p')) = 1/(1 - v^2 \cos^2 \theta_e)$.

1. Linear polarization

We evaluate the partial probabilities $w^{(lin)}(\ell)$ in Eq. (5) by a direct trace calculation of the square of the transition matrix element, similar to the case of IPA [1, 2], and express them through the generalized basis functions $\tilde{A}_m(\ell)$, which are analog of the IPA basis functions $A_m(n)$ (for circular polarization see [30]). Thus, we have

$$\begin{aligned} \frac{1}{2} w^{(lin)}(\ell) &= (2u_\ell + 1) |\tilde{A}_0(\ell)|^2 \\ &\quad - 2zu_\ell \zeta \cos \phi_e \text{Re}[\tilde{A}_0(\ell) \tilde{A}_1^*(\ell)] \\ &\quad + \xi^2 \text{Re}[\tilde{A}_0(\ell) \tilde{A}_2^*(\ell)] + \xi^2 (2u - 1) |\tilde{A}_1(\ell)|^2, \end{aligned} \quad (6)$$

where $u_\ell = u_{\max} = \ell/\zeta$. The generalized basis functions $\tilde{A}_m(\ell)$ read

$$\tilde{A}_m(\ell) = \frac{1}{2\pi} \int_{-\infty}^{\infty} d\phi \cos^m(\phi + \tilde{\phi}) e^{i\ell\phi - i\mathcal{P}^{(lin)}(\phi)} \quad (7)$$

with

$$\mathcal{P}^{(lin)}(\phi) = \tilde{\alpha}(\phi) - \tilde{\beta}(\phi), \quad (8)$$

$$\tilde{\alpha}(\phi) = \alpha \int_{-\infty}^{\phi} d\phi' f(\phi') \cos(\phi' + \phi_{CEP}), \quad (9)$$

$$\tilde{\beta}(\phi) = 4\beta \int_{-\infty}^{\phi} d\phi' f^2(\phi') \cos^2(\phi' + \phi_{CEP}),$$

$$\alpha = z \cos \phi_e, \quad \beta = \frac{u\ell\xi^2}{4u_\ell}. \quad (10)$$

The integrand of the function $\tilde{A}_0(\ell)$ in Eq. (7) does not contain the envelope function $f(\phi)$ and therefore it is

divergent. One can regularize it by using the prescription of [19] which leads to

$$\begin{aligned} \tilde{A}_0(\ell) &= \frac{1}{2\pi\ell} \int_{-\infty}^{\infty} d\phi f(\phi) e^{i\ell\phi - i\mathcal{P}^{(lin)}(\phi)} \cos(\phi + \phi_{CEP}) \\ &\quad \times (\alpha - 4\beta f(\phi) \cos(\phi + \phi_{CEP})). \end{aligned} \quad (11)$$

This equation results in the identity

$$\ell \tilde{A}_0(\ell) - \alpha \tilde{A}_1(\ell) + 4\beta \tilde{A}_2(\ell) = 0 \quad (12)$$

and allows to express the partial probability in the form

$$\begin{aligned} \frac{1}{2} w(\ell)^{(lin)} &= |\tilde{A}_0(\ell)|^2 + \xi^2 (2u - 1) \\ &\quad \times \left(|\tilde{A}_1(\ell)|^2 - \text{Re}[\tilde{A}_0(\ell) \tilde{A}_2^*(\ell)] \right), \end{aligned} \quad (13)$$

which resembles the expression for the probability in the IPA case, i.e. a monochromatic background field [2]

$$\frac{1}{2} w_n^{(lin)} = A_0^2 + \xi^2 (2u - 1) (A_1^2 - A_0 A_2), \quad (14)$$

by replacing the basis functions $\tilde{A}_m(\ell) \rightarrow A_m \equiv A_m(n\alpha\beta)$ determined as

$$A_m(n\alpha\beta) = \frac{1}{2\pi} \int_{-\pi}^{\pi} d\phi \cos^m(\phi) e^{in\phi - i\alpha \sin \phi + i\beta \sin 2\phi} \quad (15)$$

with $\beta = \beta/(1 + \xi^2/2)$ and $z = z/(1 + \xi^2/2)$, as well as with obvious substitutions $\phi_{CEP} = 0$, $\ell \rightarrow n$, $\int d\ell \rightarrow \int_{\zeta}$

$\sum_{n=n_{\min}}$, see [2] for details.

2. Circular polarization

As mentioned above, the non-linear BW process in a circularly polarized short laser pulse was considered in some detail in Refs. [14, 30, 31]. For convenience and easy reference we reproduce the main expressions of these studies. The partial probabilities are expressed through basis functions Y_ℓ, X_ℓ :

$$\begin{aligned} w^{(circ)}(\ell) &= 2|\tilde{Y}_\ell(z)|^2 + \xi^2 (2u - 1) \\ &\quad \times \left(|Y_{\ell-1}(z)|^2 + |Y_{\ell+1}(z)|^2 - 2\text{Re}(\tilde{Y}_\ell(z) X_\ell^*(z)) \right) \end{aligned} \quad (16)$$

with

$$\begin{aligned} Y_\ell(z) &= \frac{1}{2\pi} e^{-i\ell(\phi_e - \phi_{CEP})} \int_{-\infty}^{\infty} d\phi f(\phi) e^{i\ell\phi - i\mathcal{P}^{(circ)}(\phi)}, \\ X_\ell(z) &= \frac{1}{2\pi} e^{-i\ell(\phi_e - \phi_{CEP})} \int_{-\infty}^{\infty} d\phi f^2(\phi) e^{i\ell\phi - i\mathcal{P}^{(circ)}(\phi)}, \\ \tilde{Y}_\ell(z) &= \frac{z}{2\ell} (Y_{\ell+1}(z) + Y_{\ell-1}(z)) - \xi^2 \frac{u}{u_\ell} X_\ell(z), \end{aligned} \quad (17)$$

where

$$\mathcal{P}^{(circ)}(\phi) = z \int_{-\infty}^{\phi} d\phi' \cos(\phi' - \phi_e + \phi_{CEP}) f(\phi') - \xi^2 \frac{\ell u}{u_\ell} \int_{-\infty}^{\phi} d\phi' f^2(\phi'). \quad (18)$$

Equation (16) recovers the known expression for the partial probability in the IPA case [2]

$$w_n^{(circ)} = 2J_n^2(z') + \xi^2(2u-1) \times (J_{n-1}^2(z') + J_{n+1}^2(z') - 2J_n^2(z')) \quad (19)$$

by the substitutions $\ell \rightarrow n$, $|\tilde{Y}_\ell(z)|^2 \rightarrow J_n^2(z')$, $|Y_{\ell\pm 1}(z)|^2 \rightarrow J_{n\pm 1}^2(z')$, $\text{Re}(\tilde{Y}_\ell(z)X_\ell^*(z)) \rightarrow J_n^2(z')$, and $z' = (2n\xi)/(1 + \xi^2)^{1/2} \sqrt{u/u_n(1 - u/u_n)}$ with $u_n = n(k \cdot k')/2m_*^2$.

B. Numerical results

The dependence of the cross sections on the dynamic variables ξ^2 , ζ , u , and angle $\phi_{e'}$ for circular and linear polarizations is determined by the properties of the basis functions Y_ℓ , X_ℓ and $\tilde{A}_m(\ell)$, respectively. This dependence is different for the two polarizations and manifests itself in both the total and differential cross sections.

1. Total cross sections

The total cross sections as a function of the sub-threshold parameter ζ are exhibited in Fig. 1 in the upper, middle and lower panels for $\xi^2 = 10^{-4}$, 10^{-2} and 10^{-1} , respectively. The left and right panels in Fig. 1 correspond to the circular and linear polarizations, respectively. The red dashed and blue thick solid curves correspond to ultra-short and short pulses with the number of oscillations in a pulse $N = 1/2$ and 2, respectively. The thin solid curves marked by dots are for the IPA case, see (A1), i.e. a monochromatic laser background field. In both circular and linear polarizations, the theoretical model yields a step-like behavior for IPA, where each new step with ζ closest to its integer valuer n_ζ corresponds to opening a channel with the number of participating photons exceeding n_ζ , in accordance with Eq. (A1).

For finite pulses with $N \gtrsim 2$, one can see a flattening of the step-like behavior, and qualitatively they are similar to each other for both polarizations. In the case of a sub-cycle pulse with $N = 1/2$, the cross sections are greatly enhanced and they are completely smooth. No qualitative difference of linear and circular polarizations is recognizable.

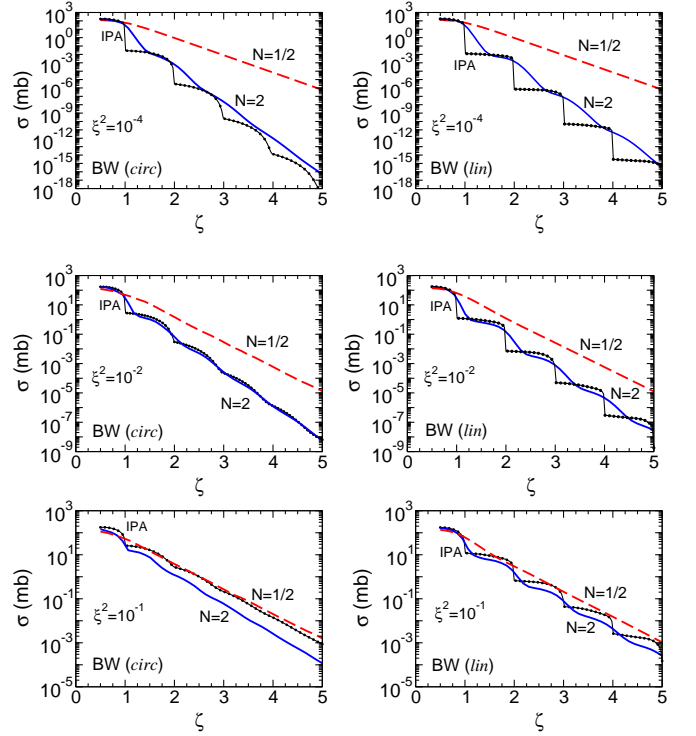


FIG. 1: (Color online) The total cross sections of the non-linear Breit-Wheeler e^+e^- -pair production as a function of the sub-threshold parameter ζ for $\xi^2 = 10^{-4}$ (top), 10^{-2} (middle) and 10^{-1} (bottom). The left and right columns correspond to the *circ* and *lin* polarizations, respectively. The red dashed and blue solid curves are for ultra-short and short pulses with number of cycles $N = 1/2$ and 2, respectively. The thin solid curves marked by dots are for the IPA case.

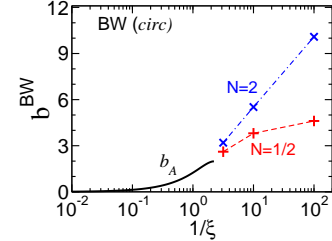


FIG. 2: (Color online) Comparison of the slopes of the exponential dependence of the cross sections $\sigma^{(circ)}(\zeta)$ as a function of $1/\xi$. The symbols + and \times are for $N = 1/2$ and 2, respectively; the thick solid curve corresponds to the asymptotic value (21).

The cross sections decrease almost exponentially with increasing ζ : $\sigma^{(i)} \propto \exp[-b^{(i)} \zeta]$, where the slopes $b^{(i)}$ depend on the pulse duration and field intensity ξ^2 . Thus, it increases with increasing pulse duration (or N) and increasing ξ . Such an exponential behavior resembles the probability of the non-linear Breit-Wheeler process in the asymptotic limit $\xi^2 \gg 1$ and $\zeta \gtrsim 2\xi^3$ [2, 30]

$$\sigma_A^{(BW)} \sim \frac{1}{\xi} \exp[-b_A \zeta], \quad (20)$$

where

$$b_A = \frac{4}{3\xi} \left(1 - \frac{1}{15\xi^2} \right). \quad (21)$$

Despite the fact that the values of ξ and ζ used in the present numerical calculations are far from their asymptotic values, in Fig. 2 we nevertheless compare for completeness the slopes obtained in our numerical calculation with their asymptotic values. The symbols + and \times are for the pulses with $N = 1/2$ and 2, respectively, and the thick solid curve corresponds to the asymptotic value given by Eq. (21). One can see a clear tendency for the numerical values of the slopes to converge their asymptotic limit.

In the asymptotic limit, the probability of e^+e^- creation for the circular polarization is greater by a factor of $(2\pi\zeta/3\xi)^{3/2}$ compared to the case of linear polarization [2]. Our numerical calculation for $\xi < 1$ is far from the asymptotic regime and results in the same order of magnitude of the e^+e^- production cross sections for circular and linear polarizations.

Finally, we note that the total cross sections shown in Fig. 1 as a function of the multi-photon (threshold) parameter ζ are determined by an interplay of two effects: (i) the multi-photon dynamics itself and (ii) the pulse shape effect. The relative contributions of these effects vary depending on the field intensity. They manifest themselves most vividly at low field intensities, where they can be separated to some extent. The first, dynamic aspect is determined by the properties of the basis functions (7), (17) and leads to a strong decrease of the cross sections as the number of photons involved in the process (or the parameter ζ) increases. The second effect is the modulation of the high-momentum components which are determined by a Fourier image of the envelope function $f(\phi)$ in (1). So, in the case of low intensities and (ultra-) short pulses, the partial probabilities as a function of ℓ are proportional to the square of $f(\ell) = \int d\phi f(\phi) \exp(-i\ell\phi)/2\pi$. The dominant contribution to the cross section (5) comes from $\ell = \zeta$ and, therefore, the shape of the cross section resembles $f^2(\ell)$ and decreases with increasing ζ . These effects – for circular polarization – are discussed in some detail in [30]. When the pulse width increases, the shape effect becomes negligible and the cross section is determined by the dynamic aspect, i.e. the properties of the basis functions, which approach the IPA basis functions for large widths (or large values of N). At intermediate field intensity ξ , there is an interplay of these two effects and it seems to be difficult to separate them. It turns out that in some cases the cross sections for finite pulses may be smaller than the IPA prediction.

2. Azimuthal angle distributions

The dependence of the differential cross sections on the azimuthal angle ϕ_e of the outgoing electron for linear and

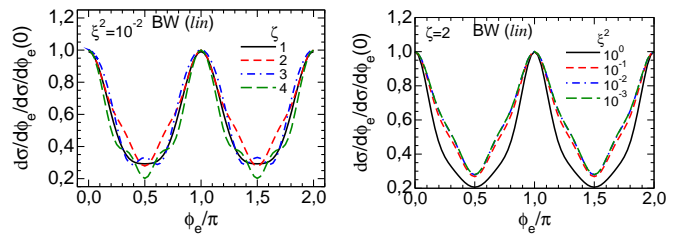


FIG. 3: (Color online) The differential cross sections $d\sigma^{(lin)}/d\phi_e$ normalized to their maximum value at $\phi_e = 0$. The left and right panels show the variation with ξ^2 and ζ , respectively, according to the legends. For *lin* polarization and IPA.

circular polarizations is mainly determined by the phase factors $\exp[-i(\ell\phi - \mathcal{P}^{(i)}(\phi))]$ in Eqs. (7) and (17), respectively. The case of circular polarization is considered in detail in [31], and therefore, below we discuss this case briefly only for completeness.

First of all note that, in the case of a circularly polarized pulse, the differential cross section in IPA does not depend on ϕ_e : it is constant and equal to $\sigma_{\text{tot}}^{(circ)}/2\pi$. In the case of linear polarization and IPA, the dependence of $d\sigma^{(lin)}/d\phi_e$ on ϕ_e exhibits a non-monotonic behavior with maxima and minima. The shape of azimuthal angle distributions is shown in Fig. 3, where the corresponding cross sections, normalized to their respective maximum value at $\phi_e = 0$, are exhibited. The left and right panels correspond to different values of e.m. field strength ξ^2 and sub-threshold parameter ζ , respectively.

Qualitatively, the reason of such a behavior is the following. The main dependence of the basis functions $A_m(n\alpha\beta)$ in (15) on $\alpha = z \cos \phi_e$ is determined by the oscillating factor in the exponent

$$A(n) \sim \frac{1}{2\pi} \int_{-\pi}^{\pi} d\phi e^{in\phi - iz \cos \phi_e \sin(\phi) + \beta \sin(2\phi)} \\ \propto \sum_k \frac{(-z \cos \phi_e)^k}{2^k k!} \int_{-\pi}^{\pi} d\phi e^{in\phi} (e^{i\phi} - e^{-i\phi})^k. \quad (22)$$

The dominant contribution to the latter sum comes from the term with $k = n$, where $n = n_{\text{min}} = \text{Int}(\zeta) \geq 1$. Here, $\text{Int}(\zeta) \equiv \lfloor \zeta \rfloor$ is the floor function which returns the maximum integer less than or equal to ζ . Since the differential cross section is a quadratic form of $A(n)$, one can estimate

$$\frac{d\sigma^{(lin)}}{d\phi_e} \propto \cos^{2n_{\text{min}}} \phi_e, \quad (23)$$

which leads to maxima at the points $\phi_e = 0, \pi$, and 2π and minima at $\phi_e = \pi/2$ and $3\pi/2$. This is in qualitative agreement with full numerical results shown in Fig. 3.

The differential cross sections for FPA and $\phi_{CEP} = 0$ are exhibited in Fig. 4. Again, in order to emphasize the shape of the distribution we present azimuthal angle

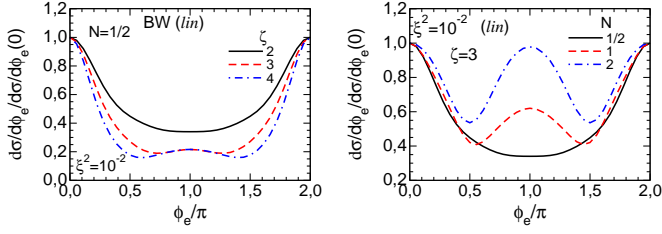


FIG. 4: (Color online) The differential cross sections $d\sigma^{(lin)}/d\phi_e$ normalized to the respective maximum value at $\phi_e = 0$ for $\xi^2 = 10^{-2}$. The left and right panels are for different values of ζ for $N = 1/2$ and for different values of N for $\zeta = 3$, respectively. For *lin* polarization and FPA and $\phi_{CEP} = 0$.

distributions of the outgoing electron $d\sigma^{(lin)}/d\phi_e$ normalized to their respective maximum value at $\phi_e = 0$.

The results for a sub-cycle pulse with $N = 1/2$ for different values of ζ are exhibited in the left panel. One can see a strong enhancement of the cross sections at $\phi_e = 0, 2\pi$ and some decrease of them when ϕ_e tends to π . Qualitatively, this is due to the fact that the oscillating factor in the basis functions $A(\ell)$ (cf. Eq. (15)) is proportional to the exponent

$$e^{i(l-z \cos \phi_e)\phi}, \quad (24)$$

with lowest oscillations and maximum contributions to the differential cross sections just at $\phi_e = 0, 2\pi$.

The right panel of Fig. 4 illustrates the evolution of the differential cross sections with increasing pulse duration (or N). The result for $N = 2$ is close to that for the IPA case (cf. Fig. 3).

The interplay of the azimuthal angle ϕ_e of the outgoing electron and the carrier envelope phase ϕ_{CEP} is interesting and important. Thus, an analysis of the corresponding angular distribution can serve as a method for the ϕ_{CEP} determination [31]. Our results for circular and linear polarizations are exhibited in Fig. 5 in the left and right panels, respectively. The calculations are performed for different pulse durations at fixed $\xi^2 = 10^{-2}$ and $\zeta = 3$.

In the case of the circular polarization, one can see a clear bump-like structure in the cross sections. The bump position coincides with the corresponding value of the carrier phase. In ultrashort pulses, the relative prominence of the bumps can reach an order of magnitude. The reason for such a behavior is that the basis functions Y_ℓ and X_ℓ are determined by the integral over $d\phi$ with a rapidly oscillating exponential function $\exp[i\Psi]$ with

$$\begin{aligned} \Psi = & l\phi - z \cos(\phi_e - \phi_{CEP}) \int_{-\infty}^{\phi} d\phi' f(\phi') \cos \phi' \\ & - z \sin(\phi_e - \phi_{CEP}) \int_{-\infty}^{\phi} d\phi' f(\phi') \sin \phi'. \end{aligned} \quad (25)$$

For short pulses, the envelope function $f(\phi)$ is essentially non-zero in the neighborhood of $\phi = 0$, and the symmetry property $f(\phi) = f(-\phi)$ holds. The integral on the sign-changing function $\sin(\phi)f(\phi)$ is much smaller than the integral on the sign-constant function $\cos(\phi)f(\phi)$ in the region of small $|\phi|$, where $f(\phi)$ is finite. This results in the inequality

$$\int_{-\infty}^{\phi} d\phi' f(\phi') \cos \phi' \gg \int_{-\infty}^{\phi} d\phi' f(\phi') \sin \phi', \quad (26)$$

which leads to the fact that the main contribution to the probability comes from the region $\phi_e \simeq \phi_{CEP}$, which is confirmed by the result of our full calculation shown in Fig. 5 (left panels). The effect of the carrier envelope phase decreases with increasing pulse duration, and for $N \geq 2$ it becomes small, where the relative height of the bumps is about 1.2 and the cross sections become close to the constant value $\sigma^{(circ)}/2\pi$.

The azimuthal angle distributions in the case of linear polarization are exhibited in the right panels of Fig. 5. The effect of a finite value of ϕ_{CEP} is most pronounced for sub-cycle pulses (cf. right top panel in Fig. 5): Similar to IPA, the cross sections have a bump at $\phi_e = \pi$. But now, the height of the bump depends on ϕ_{CEP} . It has a maximum at $\phi_{CEP} = \pi$ and becomes negligibly small

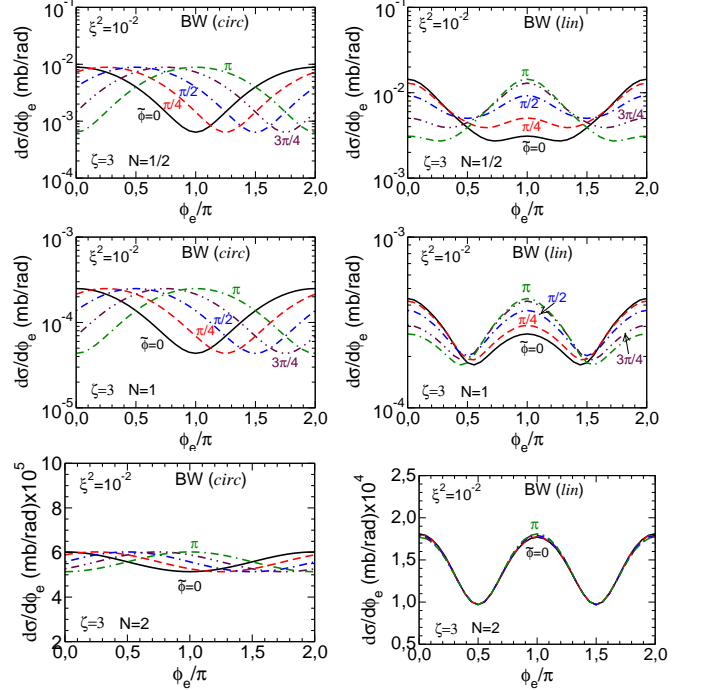


FIG. 5: (Color online) The differential cross sections $d\sigma/d\phi_e$ as a function of ϕ_e for different values of $\phi \equiv \phi_{CEP}$ for $\zeta = 3$ at $\xi^2 = 0.01$. The left and right panels are for *circ* and *lin* polarizations, respectively. The top, middle and bottom panels are for $N = 0.5, 1$ and 2 , respectively.

when $\phi_{CEP} = 0$. This is explained by the fact that the oscillation factor (24) is modified as

$$e^{i(\ell - z \cos \phi_e \cos \phi_{CEP})\phi}, \quad (27)$$

where $\phi = \mathbf{k} \cdot \mathbf{x}$ is invariant phase. This factor results in minimal oscillations of the basis functions \tilde{A}_ℓ or maximum values of cross sections for the combinations $\phi_e = 0$, $\phi_{CEP} = 0$, and $\phi_e = \pi$, $\phi_{CEP} = \pi$. Similar to the circular polarization, the impact of varying ϕ_{CEP} decreases with increasing pulse duration (or N), and at $N \gtrsim 2$ it becomes insignificant, making the differential distribution very close to the IPA prediction.

III. NON-LINEAR COMPTON SCATTERING

Compton scattering, symbolically $e^- + L \rightarrow e^- + \gamma'$, is considered here as the spontaneous emission of a photon by an electron in an external e.m. field (1). As mentioned in the introduction, the non-linear Compton process in the Furry picture is described as $e_L^- \rightarrow e_L'^- + \gamma'$. Below we use standard notations and definitions for the Compton process: the four-momenta of the incoming electron, background (laser) field (1), outgoing electron and photon are $p(E, \mathbf{p})$, $k(\omega, \mathbf{k})$, $p'(E', \mathbf{p}')$, $k'(\omega', \mathbf{k}')$, respectively. The variables $\cos \theta'$ and $\phi_{e'}$ are the polar and azimuthal angles of the outgoing photon and the outgoing electron, respectively. We consider the interaction of an initial electron with energy $E = 4$ MeV with an optical laser beam with frequency $\omega = 1.55$ eV in head-on collision geometry.

A. Basic equations

For a finite pulse, similar to the BW process, the truncated differential cross section of non-linear Compton scattering is determined by the integral of the partial contributions,

$$\frac{d\sigma^{(i)}(\kappa)}{d \cos \theta'} = \int_{\kappa}^{\infty} d\ell \frac{d\sigma_{\ell}^{(i)}}{d \cos \theta'}, \quad (28)$$

where the auxiliary continues variable ℓ appears (similarly to the variable ℓ in the BW process) in the Fourier integral of the corresponding transition matrix elements [24]. The product $\ell\omega$ has the meaning of an energy fraction of the laser beam involved in the non-linear C process. Without loss of generality, the lower limit of the integral $\kappa \equiv \ell_{\min}$ is chosen as a dynamical parameter. Its physical meaning will be discussed below. The notion ‘‘truncated differential cross section’’ implies the non-zero lower limit of the integral (28). Instead of the conventional internal Ritus variable $u = (\mathbf{k} \cdot \mathbf{k}')/(\mathbf{k} \cdot \mathbf{p}')$ with $u_{\min} = 0$ and $u_{\max} = u_{\ell} = 2\ell(\mathbf{k} \cdot \mathbf{p})/m^2$ we use the variable $\cos \theta'$ with constant limits of integration, which is

useful for the subsequent qualitative analysis and convenient for the numerical calculation of multi-dimensional integrals for total cross sections with rapidly oscillating integrands.

The differential cross section in the integrand is

$$\frac{d\sigma_{\ell}^{(i)}}{d \cos \theta'} = \frac{\alpha^2}{\xi^2 (\mathbf{p} \cdot \mathbf{k}) N_0^{(i)}} F(\ell, \cos \theta') \int_0^{2\pi} d\phi_{e'} w^{(i)}(\ell) \quad (29)$$

with

$$F(\ell, \cos \theta') = \frac{\omega'^2}{\ell\omega(E + |\mathbf{p}|)}, \quad (30)$$

where the flux factors $N_0^{(i)}$ are defined in Eq. (4). The frequency ω' of the emitted photon is related to the variable ℓ and the polar angle θ' of the direction of the momentum \mathbf{k}' through the conservation laws as

$$\omega' \equiv \omega'_{\ell} = \frac{\ell\omega(E + |\mathbf{p}|)}{E + |\mathbf{p}| \cos \theta' + \ell\omega(1 - \cos \theta')}. \quad (31)$$

The partial probabilities $w^{(i)}$ read

$$\begin{aligned} \frac{1}{2} w^{(lin)}(\ell) &= -|\tilde{A}_0(\ell)|^2 + \xi^2 \left(1 + \frac{u^2}{2(1+u)} \right) \\ &\times \left(|\tilde{A}_1(\ell)|^2 - \text{Re} \tilde{A}_0(\ell) \tilde{A}_2^*(\ell) \right), \quad (32) \end{aligned}$$

$$\begin{aligned} w^{(circ)}(\ell) &= -2|\tilde{Y}_{\ell}(z)|^2 + \xi^2 \left(1 + \frac{u^2}{2(1+u)} \right) \times \\ &\left(|Y_{\ell-1}(z)|^2 + |Y_{\ell+1}(z)|^2 - 2\text{Re}(\tilde{Y}_{\ell}(z) X_{\ell}^*(z)) \right). \quad (33) \end{aligned}$$

The basis functions $\tilde{A}(\ell)$, and Y_{ℓ} , X_{ℓ} and $\tilde{Y}_{\ell}(z)$ are defined in Eqs. (7) and (17), respectively. For the dynamical variable z we use the standard definition $z = 2\ell\xi((u/u_{\ell})(1 - u/u_{\ell}))^{1/2}$. The partial probabilities $w^{(i)}$ resemble the corresponding expressions in the IPA (cf. Eqs. (A3) and (A4)).

Evaluating Eq. (28), we express first the variable u in the partial probabilities through $\cos \theta'$ in c.m.s. ($\cos \theta'_c$) as $u = \omega_c(1 - \cos \theta'_c)/(E_c + \omega_c \cos \theta'_c)$ with $\omega_c = \ell(\mathbf{p} \cdot \mathbf{k})/2\sqrt{s}$, $E_c = (s + m^2)/2\sqrt{s}$ and then express $\cos \theta'_c$ via $\cos \theta'$ in the lab. system as $\cos \theta'_c = (v - \cos \theta')/(v \cos \theta' - 1)$ with $v = -(|\mathbf{p}| - \ell\omega)/(E + \ell\omega)$.

Often, analysis of the non-linear C process is constrained entirely to the energy (ω') and angular (θ' and ϕ') distributions of the outgoing photon. Our approach here allows for an easy access to the polar photon angle θ' and the azimuthal final-state electron angle $\phi_{e'}$. Such a mixed phase space distribution is to be contrasted with analyses which focus entirely on the kinematics of the outgoing electron [43].

Now, we would like to stress that the differential cross section (28) with (29) for $\ell > 1$ has a sharp maximum in the backward hemisphere in the vicinity of

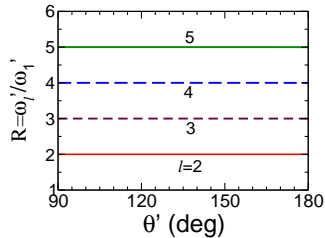


FIG. 6: (Color online) The ratio $R = \omega'_\ell/\tilde{\omega}'_1$ as a function of θ' for different values of ℓ .

$\theta' = \theta'_0 \simeq 175^\circ$, similar to that in the case of IPA (cf. Fig. 13 below). A sharp increase of the cross section in the backward hemisphere is a well-known property of Compton scattering [12]. In the case of non-linear Compton scattering, when a finite number of background field photon modes contribute, a sharp maximum appears [13], the position of which depends on initial-state kinematics and is less sensitive to the field intensity, at least for $\xi^2 < 10$ (cf. A 2).

In a practical study of the Compton scattering, one can choose another angle $\theta' < \theta'_0$ (in accordance with the experimental set-up), remembering that (i) the cross section in this case will be smaller, and (ii) qualitatively the main results do not depend on the choice of this angle.

Discussing the physical meaning of the dynamical parameter κ it is convenient to consider the ratio $R(\ell, \theta') = \omega'_\ell/\omega'_1$, where ω'_1 is the frequency of the photon emitted in the interaction of an initial electron with a single photon of the pulse at the same angle

$$\omega'_1 = \frac{\omega(E + |\mathbf{p}|)}{E + |\mathbf{p}| \cos \theta' + \omega(1 - \cos \theta')} . \quad (34)$$

The ratio R as a function of θ' in the backward hemisphere for the chosen kinematics is exhibited in Fig. 6 for different values of ℓ . It can be seen that R is practically independent of θ' . Thus, the relation between R , ℓ and θ' reads

$$R = \frac{\ell}{1 + \delta(\ell - 1)} , \quad (35)$$

where

$$\delta = \varepsilon \frac{1 - \cos \theta'}{1 + v_e \cos \theta' + \varepsilon(1 - \cos \theta')} \quad (36)$$

with $\varepsilon = \omega/E$ and $v_e = |\mathbf{p}|/E$. For the chosen kinematics, $\varepsilon \simeq 3.85 \times 10^{-7}$ and δ varies from 3.8×10^{-7} to 9.5×10^{-5} when θ' varies from $\pi/2$ to π , respectively. Therefore, with great accuracy, the lower limit of the integral in (28) may be chosen as $\kappa = \ell_{\min} = R = \omega'/\omega'_1$ in a wide interval of θ' in the backward hemisphere. As mentioned above, the product $\ell\omega$ has the meaning of the pulse energy involved into the process. The multi-photon dynamics refers to $\ell > 1$. Since in our definition

$\ell_{\min} = \kappa$, the cross section $\sigma(\kappa)$ with $\kappa > 1$ corresponds to the multi-photon Compton regime. This is the physical meaning of $\kappa > 1$ as a value reflecting the onset of multi-photon dynamics.

In order to isolate multi-photon events, one has to install a detector at fixed polar angle θ' and register only such photons with the frequencies higher than ω'_κ (or $\omega' \geq \omega'_\kappa$) with $\kappa > 1$. A preferred angle of detection is in the backward hemisphere, where the cross section is significantly larger.

Recall that the cross sections (28) are integrated over the azimuthal angle $\phi_{e'}$. This means that a selection of multi-photon events would be performed as a sum of events in the interval $0 \geq \phi_{e'} \geq \pi$ with an appropriate binning (where we assume the symmetry of the azimuthal angle distribution with respect to the substitution $\phi_{e'} \rightarrow 2\pi - \phi_{e'}$). Technically, a corresponding measurement seems to be quite feasible, especially since our subsequent study implies exactly the same analysis of azimuthal angle distributions. However, bearing in mind that the frequencies of outgoing photons ω'_κ and ω'_1 , respectively, are independent of $\phi_{e'}$, the conclusion about the physical meaning of $\kappa > 1$ as a suitable starting point of switching on the corresponding multi-photon regime remains appropriate. On the other hand, the favorable intervals for the study of the azimuthal angle distribution may be understood from our analysis of the corresponding azimuthal angle distributions given below in subsection 2. For IPA and *circ* polarization, the problem is simplified since the azimuthal angle distribution is isotropic in this case.

B. Numerical results

The dependences of the non-linear C process on the variables ℓ , z u and the field strength ξ^2 for *lin* and *circ* polarizations are realized through the basis functions $\tilde{A}_m(\ell)$ and Y_ℓ , X_ℓ , respectively and, in general, are different for these two cases, both for the truncated total cross sections and for the differential distributions.

1. Truncated total cross section

The truncated total cross sections integrated over $d \cos \theta'$ ¹

$$\sigma^{(i)}(\kappa) = \int_{\kappa}^{\infty} d\ell \int_{-1}^1 d \cos \theta' \int_0^{2\pi} d\phi_{e'} \frac{d\sigma_\ell^{(i)}}{d\phi_{e'} d \cos \theta'} , \quad (37)$$

¹ The notion of a “truncated cross section” is to emphasize that we are employing a non-zero lower limit of the integration, $\ell_{\min} = \kappa$. The phrase “partially integrated cross section” is also suitable for the distinction to the total cross section integrated over the full out-phase space.

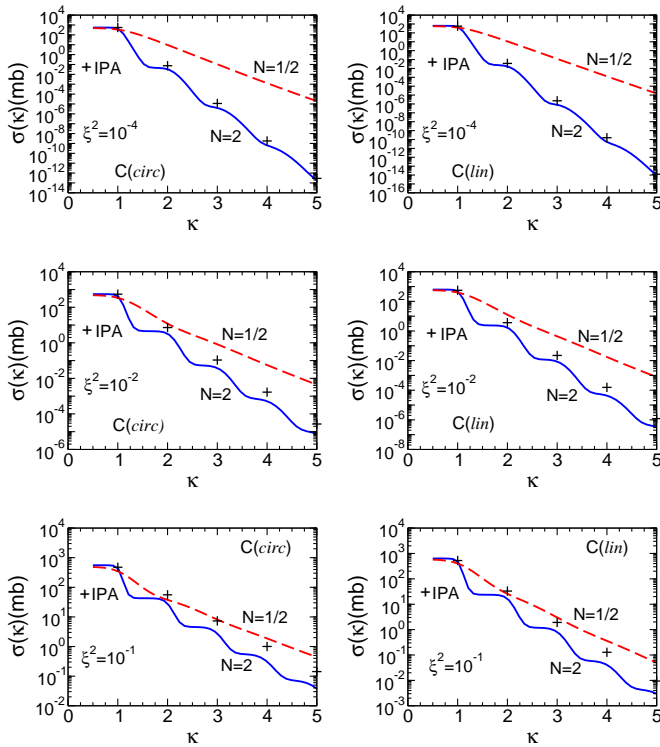


FIG. 7: (Color online) The truncated cross sections $\sigma(\kappa)$ as a function of the parameter κ at $\xi^2 = 10^{-4}$ (top), 10^{-2} (middle) and 10^{-1} (bottom). The left and right columns correspond to the *circ* and *lin* polarizations, respectively. The dashed and thick solid curves are for ultra-short and short pulses with the number of cycles $N = 1/2$ and 2 , respectively. The crosses are for the IPA. The minimal values of corresponding harmonics are chosen as integer parts of κ .

as a function of the threshold parameter κ at e.m. field strength parameters $\xi^2 = 10^{-4}$, 10^{-2} and 10^{-1} are shown in Fig. 7 in the upper, middle and lower panels, respectively. The left and right panels correspond to the circular and linear polarizations, respectively. Remembering that the multi-photon regime arises at $\kappa > 1$, for completeness we extend our consideration to smaller values $\kappa \geq 0.5$ and $n_{\min} \geq 1$. The dashed and thick solid curves correspond to the ultra-short and short pulses with the number of oscillations $N = 1/2$ and 2 , respectively. The crosses are for the IPA. The values of corresponding minimum number of harmonics n_{\min} in Eq. (A2) are chosen as integer parts of κ . At $\kappa \approx 1$, where only one photon from the pulse participates, the results of all calculations are very close to each other. The cross sections decrease for increasing κ . In the case of $N = 2$, the shape of the curves resembles the step-like behavior. For the sub-cycle pulse with $N = 1/2$ the cross sections decrease exponentially with κ , $\sigma \propto \exp[-b^{(i)}\kappa]$. The slopes $b^{(i)}$ depend on the field intensity and, in general, on the polarization. In the case of linear polarization, the slope $b^{(lin)}$ is larger.

Note that the exponential decrease of the total cross sections as a function of κ has the same reason as in the case of the non-linear BW process (cf. Fig. 1), where

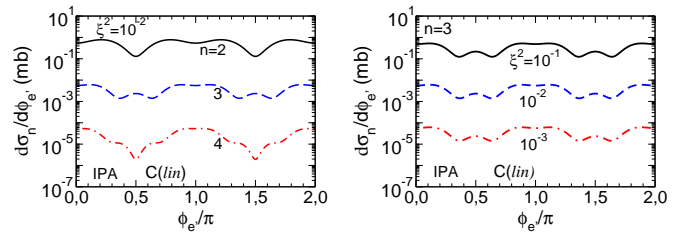


FIG. 8: (Color online) The differential cross sections $d\sigma_n^{(lin)}/d\phi_{e'}$ in IPA. The left and right panels correspond to calculations for various values of harmonic number n at $\xi^2 = 10^{-2}$ and for various values of ξ^2 at $n = 3$, respectively.

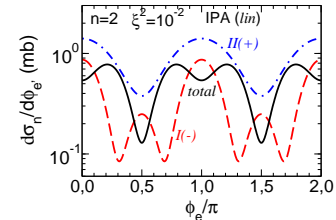


FIG. 9: (Color online) The differential cross sections of the non-linear C process in IPA for the harmonic $n = 2$ and $\xi^2 = 10^{-2}$ together with the separate contributions of the first $I(-)$ and second $II(+)$ terms in the partial probability (A3). The thick solid curve is for the coherent sum of both contributions.

the cross sections are functions of ζ . Now, the threshold parameter κ is an analog of the parameter ζ and the previous discussion at the end of Sect. III.B applies to the non-linear Compton scattering, considered here.

2. Azimuthal angle distributions

Analog to the non-linear BW process, the shape of the differential cross sections as a function of the azimuthal angle $\phi_{e'}$ of non-linear C scattering for linear and circular polarizations is determined mainly by the phase factors $\mathcal{P}^{(i)}$ in Eqs. (8) and (18), respectively. Again, for a monochromatic circularly polarized beam (IPA case), the differential cross section does not depend on $\phi_{e'}$.

In the case of linear polarization, the azimuthal angle distribution (in IPA) shown in Fig. 8 exhibits non-monotonic behavior. For example, in the case of $n = 2$ and $\xi^2 = 10^{-2}$, one sees some local minima at $\phi_{e'} = 0, \pi$ and 2π , some deepening at $\phi_{e'} = \pi/2, 3\pi/2$ and bumps at $\phi_{e'} = \pi/4, 3\pi/4, 5\pi/4$ and $7\pi/4$. The left and right panels of Fig. 8 correspond to calculations for different harmonic numbers n at $\xi^2 = 10^{-2}$ and different values of ξ^2 at $n = 3$, respectively. All cross sections are symmetric under the transformation $d\sigma_n(\phi_{e'}) \rightarrow d\sigma_n(2\pi - \phi_{e'})$.

The reason of the non-monotonic shape of distributions is the destructive interference of the first and second terms in the partial probability in Eq. (A3). Thus, Fig. 9

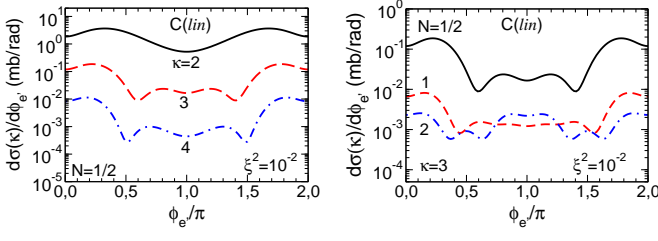


FIG. 10: (Color online) The differential cross sections $d\sigma^{(lin)}(\kappa)/d\phi_{e'}$ at $\xi^2 = 10^{-2}$. The left and right panels are for calculations at $N = 1/2$ and different values of κ and for different values N at $\kappa = 3$, respectively.

exhibits the differential cross section of the non-linear C process at $n = 2$ and $\xi^2 = 10^{-2}$ together with separate contributions of the first (*I*) and second (*II*) terms in the partial probability in Eq. (A3). One can see that, at points at $\phi_{e'} = 0, \pi$ and 2π , the absolute values of (*I*) and (*II*) are close to each other and, being opposite in sign, they mutually compensate each other. At the points $\phi_{e'} = \pi/4, 3\pi/4, 5\pi/4$ and $7\pi/4$, the contribution of the first term is negligible which leads to certain local maxima. At the points $\phi_{e'} = \pi/2$ and $3\pi/2$, one can also observe some local compensation of the two terms which leads to the corresponding deepening in the distribution. However, the depth of these local minima is less than in the first case and, generally, depends on the values of n and ξ^2 .

The differential distributions for linear polarization and in FPA with $\phi_{CEP} = 0$ are exhibited in Fig. 10. The left and right panels correspond to calculations at different values of the parameter κ for $\xi^2 = 10^{-2}$ and $N = 1/2$, and to different values of the pulse duration at the same value ξ^2 and $\kappa = 3$, respectively. Again, one can see a non-monotonic shape and a multi-bump structure of the distributions, which is a consequence of the interference of the two terms in the partial probabilities of Eq. (32). The shapes are different from that in the case of a circularly polarized pulse [31].

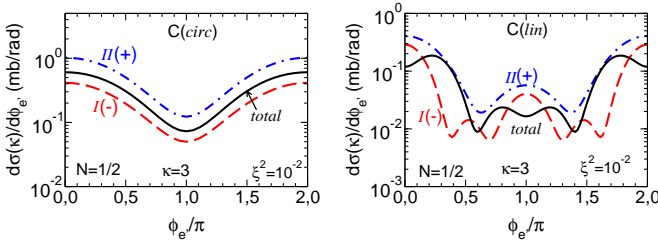


FIG. 11: (Color online) The differential cross sections $d\sigma(\kappa)/d\phi_{e'}$ at $N = 1/2$, $\xi^2 = 10^{-2}$ and $\kappa = 3$. The left and right panels are for *circ* and *lin* pulse polarizations, respectively. The dashed and dot-dashed curves labeled by *I*(-) and *II*(+) are for the first (negative) and second terms in Eqs. (32), (33), respectively. The thick solid curve is for the coherent sum of both contributions.

In fact, for both circular and linear polarizations, the

total probability is a coherent sum of negative and positive terms in the partial distributions in Eqs. (32) and (33). But the azimuthal angle dependencies of these two terms are either similar or quite different for *circ* or *lin* pulse polarizations, respectively, which is illustrated in the left and right panels of Fig. 11. As a result, the azimuthal angle distributions have either one bump at $\phi_{e'} = 0 (2\pi)$ or a multi-bump structure for *circ* or *lin* polarizations, respectively.

Manifestations of the interplay of the azimuthal angle of the outgoing electron $\phi_{e'}$ and the carrier envelope phase ϕ_{CEP} for the non-linear Compton scattering in the azimuthal angle distribution in the case of finite pulses are shown in Fig. 12. The results for circular and linear polarizations are exhibited in the left and right panels, respectively. The calculations are for fixed values $\kappa = 3$ and $\xi^2 = 10^{-2}$ and for different pulse durations with $N = 1/2, 1$ and 2 exhibited in the top, middle and bottom panels, respectively.

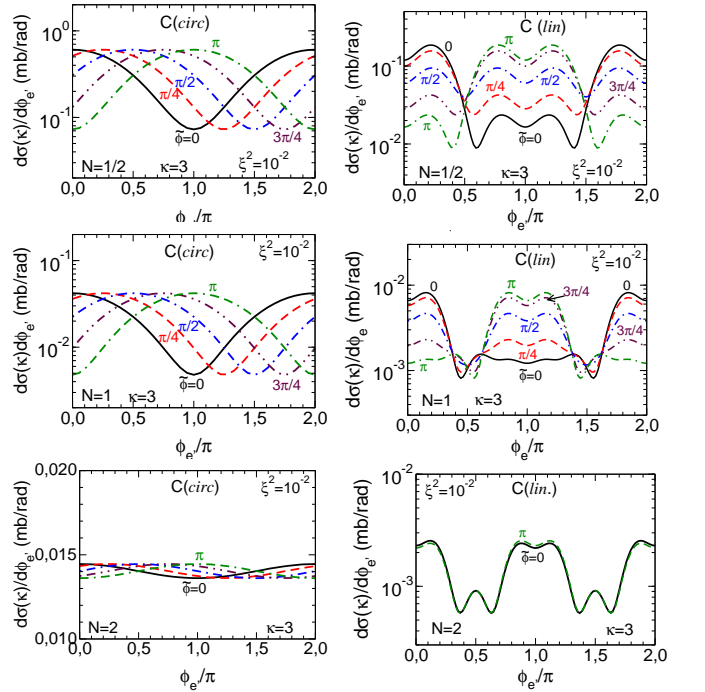


FIG. 12: (Color online) The differential cross sections $d\sigma(\kappa)/d\phi_{e'}$ as a function of $\phi_{e'}$ for different values of $\tilde{\phi} \equiv \phi_{CEP}$ for $\kappa = 3$ and $\xi^2 = 10^{-2}$. The left and right panels are for circular and linear polarizations, respectively. The top, middle and bottom panels are for $N = 1/2, 1$ and 2 , respectively.

Similar to the non-linear Breit-Wheeler process, in the case of circular polarization, the shapes of the distributions are smooth curves with maxima and minima at the points $\phi_{e' \max} = \phi_{CEP} \pm 2\pi$ and $\phi_{e' \min} = \phi_{e' \max} \pm \pi$. The explanation for this behavior is the same as in the case of the non-linear Breit-Wheeler process discussed in Sect. III. The shapes of the distributions are similar for different pulse durations ranging from $N = 1/2$ to

$N = 2$. However, the relative amplitude of the oscillations, $d\sigma(\phi_{e'_{\max}})/d\sigma(\phi_{e'_{\min}})$, changes from about 23 at $N = 1/2$ to about 1.06 at $N = 2$. This means that for $N \gtrsim 2$ the azimuthal angle distributions can be considered as isotropic.

For the linear polarization, the situation is quite different. As pointed out above, in the case of $\phi_{CEP} = 0$, one gets the results already discussed above. The angular distributions $d\sigma_0(\kappa)/d\phi_{e'}$ have maxima at $\phi_{e'} = \pi/4, 3\pi/4, 5\pi/4$ and $7\pi/4$. For sub-cycle and short pulses the height of the first (second) bump increases when ϕ_{CEP} decreases (increases). That is because the phase factor in the basis functions $\tilde{A}_m(\ell)$ in Eq. (7) is determined by the highly oscillating function $\int dx \exp[-i(\ell x - \mathcal{P}^{(lin)})]$ depending on the product $c = \cos \phi_{e'} \cos \phi_{CEP}$, thus enhancing the cross section for positive values of c . A closer inspection leads to the bump positions $\phi_{e'} = \pi/4, \phi_{CEP} = 0, \phi_{e'} = 3\pi/4, \phi_{CEP} = \pi$ and so on. At $\phi_{CEP} = \pi/2$, the height of the bumps does not depend on the bump position. Note that the factor c does not determine directly the bump positions, which depend also on the interplay of the two terms in the partial probability (32).

For relatively long pulse with $N \gtrsim 2$, similarly to the case of circular polarization, the angular distribution does not depend on ϕ_{CEP} , but in contrast to the circular polarization now it is not isotropic and it becomes close to the IPA result (cf. Fig. 8).

IV. SUMMARY

In summary we have performed a simultaneous analysis of two essentially non-linear QED processes in circularly and linearly polarized short and intensive e.m. (laser) pulses: (i) non-linear Breit-Wheeler e^+e^- pair creation in the interaction of a probe photon with such a pulse and (ii) the photon emission or the non-linear Compton scattering when an initial electron interacts with the short and intensive e.m. (laser) pulse. Both processes are analyzed in the multi-photon region, where several photons participate at the same time. In the case of non-linear Breit-Wheeler e^+e^- pair emission, the multi-photon region is determined uniquely by the threshold variable $\zeta > 1$ or $s < s_{\text{thr}} = 4m^2$. For the non-linear Compton scattering, we use the partially integrated (i.e. truncated) cross section, where the integration starts from the dynamical parameter $\kappa > 1$ which selects the multi-photon events and is an analog of the variable ζ in the non-linear Breit-Wheeler process.

Our analysis shows a step like dependence of the total cross sections of ζ (κ) for the non-linear Breit-Wheeler (Compton) process in the case of relatively long pulses with the number of oscillations in a pulse $N \gtrsim 2$, similar to the prediction for the infinitely long pulse. In the case of a sub-cycle pulse ($N = 1/2$), the cross sections exhibit an exponential dependence $\exp[-b_\zeta \zeta]$ ($\exp[-b_\kappa \kappa]$). The slopes b_ζ, b_κ depend on the field intensity and the pulse duration.

The azimuthal angle distributions are very sensitive to the choice of parameters and, in particular, depend on the carrier envelope phase ϕ_{CEP} . In addition to the processes occurring in the circularly polarized e.m. pulses considered earlier [31], the case of linear polarization leads to a qualitative modification of the azimuthal distributions of outgoing electrons. These distributions are non-monotonic functions with peculiar maxima and minima. In most cases we gave qualitative explanations of their positions which are confirmed by the exact numerical calculations. Their positions, heights, and depths are determined by the structure of the phase factor $\mathcal{P}^{(lin)}$ of the basis functions \tilde{A}_m , which in turn depend on the dynamic variables ξ^2, ζ, κ , and the carrier envelope phase ϕ_{CEP} and the pulse width (Δ) as well. In the case of non-linear Compton scattering, the angular distributions are determined by a nontrivial destructive interference of the terms in the partial probability $w^{(lin)}(\ell)$. This result depends on the pulse duration: for pulses with $N \gtrsim 2$, the dependence of the azimuthal angle distributions on the CEP disappears.

The effects of the ϕ_{CEP} imprint on azimuthal angle distributions in the considered processes are comparable with predictions of CEP phenomena in other processes involving ultrashort laser pulses [36–38], such as CEP manifestations in the polar angular distributions of positrons in the BW processes [29], electron tunneling in a coupled double-quantum-dot system [41], and strong-field ionization [42]. Our results in Sect. III.B.2 may be compared with that for non-linear Compton scattering of recent Refs. [39, 40], where the polar angular distribution of outgoing electrons is analyzed, and it is found that the distributions have some sharp peaks, the positions and heights of which depend on ϕ_{CEP} . Thus, the height of the peaks is modified by a factor ≈ 1.8 when ϕ_{CEP} changes from 0 to π . This result can be compared with our prediction of interference effects in azimuthal angle distributions exhibited in Fig. 12 (upper panels) where, e.g. for $N = 1/2, 1$ and $\phi_{e'} = 0$, the cross section is modified by an order of magnitude for the ϕ_{CEP} varying from 0 to π . However, we have to stress that our result and the results of [39, 40] for relatively long pulses are obtained for quite different initial conditions $\gamma \gg \xi$ vs. $\gamma \ll \xi$, respectively, where γ is the Lorentz factor of the incoming electron. Therefore, the chosen observables and the specific initial conditions are very important for a ϕ_{CEP} determination.

Our theoretical predictions for circularly and linearly polarized laser pulses may be used as a unique and powerful input for the design of forthcoming experiments in the near future and corresponding experimental studies of different aspects of the multi-photon dynamics related to non-linear QED processes and, in particular, for a ϕ_{CEP} determination.

Acknowledgments

The authors gratefully acknowledge the collaboration with D. Seipt, T. Nusch, T. Heinzl, and useful discussions with A. Ilderton, K. Krajewska, M. Marklund, C. Müller, and R. Schützhold. A. Ringwald is thanked for explanations w.r.t. LUXE. The work is supported by R. Sauerbrey and T. E. Cowan w.r.t. the study of fundamental QED processes for HIBEF.

Contributions

All authors have contributed equally to the publication, being variously involved in the conceptual outline, software development and numerical evaluations.

Appendix A: Multi-photon regime in IPA

1. Breit-Wheeler process

The cross sections of the non-linear BW process in IPA as a function of $s = 4m^2/\zeta$ are represented by an infinite sum of harmonics labeled by n (cf. [44])

$$\sigma^{(i)}(s) = \frac{\alpha^2 \zeta}{4m^2 \xi^2 N_0^{(i)}} \times \sum_{n=n_{\min}}^{\infty} \int_0^{2\pi} d\phi_e \int_1^{u_n} \frac{du}{u^{3/2} \sqrt{u-1}} w_n^{(i)} \quad (\text{A1})$$

with $N_0^{(lin)} = 1/2$ and $N_0^{(circ)} = 1$, and the partial harmonics $w^{(i)}$ determined by Eqs. (14) and (19), respectively. The minimum number n is determined as the integer part (Int) of $\zeta = 4m^2/s$: in detail, $n_{\min} = \text{Int}(\zeta)$ if $\text{Int}(\zeta) = \zeta$ and $n_{\min} = \text{Int}(\zeta) + 1$ if $\text{Int}(\zeta) < \zeta$. So, for example, for the above-threshold process with $\zeta < 1$, one has $n_{\min} = 1$.

2. Compton scattering

The total cross sections in IPA are expressed in standard notation as an infinite sum of harmonics labeled by n [12]

$$\sigma^{(i)} = \frac{\alpha^2}{\xi^2(p \cdot k) N_0^{(i)}} \times \sum_{n=1}^{\infty} \int_0^{2\pi} d\phi_{e'} \int_0^{u_n} \frac{du}{(1+u)^2} w_n^{(i)}, \quad (\text{A2})$$

where $N_0^{(i)}$ is defined below Eq. (A1), and $u_n = 2n(p \cdot k)/m_*^2$. The physical meaning of the quantity n is as fol-

lows. It is the number of photons of the laser beam participating in the process with the formation of a photon with frequency ω' . The product $n\omega$ is the energy fraction of the background field involved into the process.

The partial probabilities (harmonics) in Eq. (A2) for *lin* and *circ* polarizations read

$$\frac{1}{2} w_n^{(lin)} = -A_0^2 + \xi^2 \left(1 + \frac{u^2}{2(1+u)} \right) (A_1^2 - A_0 A_2) \quad (\text{A3})$$

and

$$w_n^{(circ)} = -2J_n^2 + \xi^2 \left(1 + \frac{u^2}{2(1+u)} \right) \times (J_{n-1}^2 + J_{n+1}^2 - 2J_n^2), \quad (\text{A4})$$

where the notations for the basis functions are the same as in Sect. III (see Eqs. (14) and (19) for details). Naturally, in the case of IPA one has to use kinematics, conservation laws and dynamical variables u, z for dressed fermions [2].

Selecting multi-photon processes with $n > 1$ from the infinite sum (A2) may be done similarly to that given in Sect. IV. First, we express the cross sections (A2) in an equivalent but slightly different form

$$\sigma^{(i)} = \sum_{n=1}^{\infty} \int_{-1}^1 d \cos \theta' \frac{d\sigma_n^{(i)}}{d \cos \theta'}, \quad (\text{A5})$$

where $d\sigma_n^{(i)}/d \cos \theta'$ is the differential cross section for each separate harmonic

$$\frac{d\sigma_n^{(i)}}{d \cos \theta'} = \frac{\alpha^2}{\xi^2(p \cdot k) N_0^{(i)}} F_n \int_0^{2\pi} d\phi_{e'} w_n^{(i)} \quad (\text{A6})$$

with $F_n = \omega_n'^2/n(p \cdot k)$. The frequency of an outgoing photon emitted at polar angle θ' reads for the n th harmonic in IPA

$$\omega_n' = \frac{n\omega(E + |\mathbf{p}|)}{E + |\mathbf{p}| \cos \theta' + \omega(n + \frac{\xi^2 m^2}{2\lambda(k \cdot p)})(1 - \cos \theta')}, \quad (\text{A7})$$

where $\lambda = 1$ or 2 for *circ* or *lin* polarizations, respectively.

The differential cross sections (A6) for the individual harmonics with $n = 1 \dots 5$ and $\xi^2 = 10^{-1}$ are shown in Fig. 13. The left and right panels are for circularly and linearly polarized beams, respectively. The initial electron energy and the frequency of the photon beam (in lab. system) are 4 MeV and 1.55 eV, respectively. The crosses are for the Klein-Nishina result [12]. One can see that the harmonic $n = 1$ at $\xi^2 \leq 0.1$ fairly well reproduces the Klein-Nishina cross section for $\gamma + e \rightarrow \gamma' + e'$. In the case of multi-photon processes with $n > 1$, the calculation predicts a strong bump in the backward hemisphere which seems to be preferable to study the multi-photon

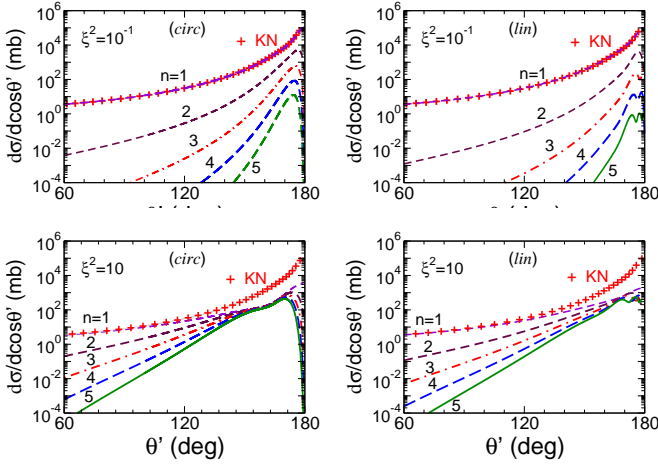


FIG. 13: (Color online) The differential cross sections for the individual harmonics (cf. Eq. (A6)) with $n = 1 \dots 5$ (according to legend) and $\xi^2 = 10^{-1}$ (top panels) and 10 (bottom panels). The crosses are for the Klein-Nishina cross section. The left and right panels are for *circ* and *lin* polarizations, respectively. The electron energy and the frequency of the photon beam (in lab. system) are 4 MeV and 1.55 eV, respectively. Note the dead cone for harmonics $n > 1$, i.e. no on-axis backscattering, for *circ* polarization, while for *lin* polarization, the odd-number harmonics are backscattered on-axis.

processes (cf. our discussion in Sect. IV.A). Closer inspection of the cross sections for linear polarization in the vicinity of $\theta' = \pi$ shows that they are finite for odd harmonics and equal to zero for even harmonics (the so called "dead cone behavior", cf. [13]). For circular polarization, the cross sections are equal to zero at $\theta' = \pi$ for all higher harmonics with $n > 1$.

In order to select essentially multi-photon interactions the summation in (A2) should start from $n = \hat{n}$ equal to ω'/ω'_1 , which coincides with the integer part of the ratio $\kappa = \omega'/\omega'_1$ in the case of FPA.

-
- [1] A. I. Nikishov and V. I. Ritus. "Quantum processes in field of a plane electromagnetic wave and a constant field". Sov. Phys. JETP. **19**, 529 (1964); N. V. Narozhny, A. I. Nikishov, and V. I. Ritus. "Quantum processes in field of a circularly polarized electromagnetic wave". Sov. Phys. JETP. 1965. **20**, 622-629.
- [2] V. I. Ritus. "Quantum effects of the interaction of elementary particles with an intense electromagnetic field". J. Sov. Laser Res. (United States), **6:5**, 497 (1985).
- [3] H. R. Reiss. "Absorption of Light by Light". J. Math. Phys. **3**, 59 (1962); H. R. Reiss. "Production of electron pairs from a zero-mass state". Phys. Rev. Lett. **26**, 1072 (1971).
- [4] G. A. Mourou, T. Tajima, and S. V. Bulanov. "Optics in the relativistic regime". Rev. Mod. Phys. **78**, 309 (2006).
- [5] A. Di Piazza, C. Müller, K. Z. Hatsagortsyan, and C. H. Keitel. "Extremely high-intensity laser interactions with fundamental quantum systems". Rev. Mod. Phys. **84**, 1177 (2012).
- [6] N. B. Narozhny and A. M. Fedotov. "Extreme light physics". Contemp. Phys. **56**, 249 (2015).
- [7] K. Homma, D. Habs, G. Mourou, H. Ruhl, T. Tajima. "Opportunities of fundamental physics with high-intensity laser fields". Prog. Theor. Phys. Suppl. **193**, 224 (2012).
- [8] A. Di Piazza, M. Tamburini, S. Meuren, C.H. Keitel. "Improved local-constant-field approximation for strong-field QED codes". Phys. Rev. A **99**, 022125, (2019).
- [9] A. Ilderton, B. King and D. Seipt, "Extended locally constant field approximation for nonlinear Compton scattering". Phys. Rev. A **99**, 042121 (2019).
- [10] D. Seipt. "Volkov States and Non-linear Compton Scattering in Short and Intense Laser Pulses". arXiv:1701.03692 [physics.plasm-ph].
- [11] D. Y. Ivanov, G. L. Kotkin and V. G. Serbo, "Complete description of polarization effects in e+e- pair production by a photon in the field of a strong laser wave". Eur. Phys. J. C **40**, 27 (2005).
- [12] V. B. Berestetskii, E. M. Lifshitz, and L. P. Pitaevskii. "Quantum Electrodynamics", 2nd ed., Course of Theoretical Physics, Vol. 4 (Pergamon, Oxford, New York, 1982).
- [13] C. Harvey, T. Heinzl and A. Ilderton, "Signatures of High-Intensity Compton Scattering". Phys. Rev. A **79**, 063407 (2009).
- [14] A. I. Titov, B. Kämpfer, A. Hosaka and H. Takabe. "Quantum processes in short and intensive electromagnetic fields". Phys. Part. Nucl. **47**, 456 (2016).
- [15] D. L. Burke, *et al.*. "Positron Production in Multiphoton Light-by-Light Scattering". Phys. Rev. Lett, **79**, 1626 (1997); C. Bamber, *et al.*. "Studies of nonlinear QED in collisions of 46.6 GeV electrons with intense laser pulses". Phys. Rev. D. **60**, 092004(1999).
- [16] M. Altarelli *et al.* "Summary of strong-field QED Workshop", arXiv:1905.00059 [hep-ex].
- [17] A. Hartin, A. Ringwald and N. Tapia. "Measuring the Boiling Point of the Vacuum of Quantum Electrodynamics". Phys. Rev. D **99**, 036008 (2019).
- [18] F. Mackenroth and A. Di Piazza. "Non-linear Compton scattering in ultra-short laser pulses". Phys. Rev. A **83**, 032106 (2011).
- [19] M. Boca and V. Florescu. "Non-linear Compton scattering with a laser pulse". Phys. Rev. A **80**, 053403 (2009), Erratum Phys. Rev. A **81**, 039901 (2010).

- [20] M. Boca and V. Florescu. "Electron distributions in non-linear Compton scattering". *Phys. Rev. A* **86**, 013414 (2012).
- [21] K. Krajewska, and J. Z. Kaminski. "Compton process in intense short laser pulses". *Phys. Rev. A* **86**, 062102 (2012).
- [22] T. Heinzl, D. Seipt, and B. Kämpfer. "Beam-shape effects in non-linear Compton and Thomson scattering". *Phys. Rev. A* **81**, 022125 (2010).
- [23] F. Mackenroth, A. Di Piazza, and C. H. Keitel. "Determining the Carrier-Envelope Phase of Intense Few-Cycle Laser Pulses". *Phys. Rev. Lett.* **105**, 063903, (2010).
- [24] A. I. Titov, B. Kämpfer, T. Shibata, A. Hosaka and H. Takabe. "Laser pulse-shape dependence of Compton scattering". *Eur. Phys. J. D* **68**, 299 (2014).
- [25] D. Seipt and B. Kämpfer. "Asymmetries of azimuthal photon distributions in non-linear Compton scattering in ultra-short intense laser pulses". *Phys. Rev. A* **88**, 012127 (2013).
- [26] V. Dinu, T. Heinzl, and A. Ilderton. "Infra-Red Divergences in Plane Wave Backgrounds". *Phys. Rev. D* **86**, 085037 (2012).
- [27] K. Krajewska, F. Cajiao Vlez, and J. Z. Kaminski. "Generalized Klein-Nishina formula". *Phys. Rev. A* **91**, 062106 (2015).
- [28] T. Nusch, D. Seipt, B. Kämpfer and A. I. Titov. "Pair production in short laser pulses near threshold". *Phys. Lett. B* **715**, 246 (2012).
- [29] K. Krajewska, and J. Z. Kaminski. "Breit-Wheeler Process in Intense Short Laser Pulses". *Phys. Rev. A* **86**, 052104 (2012).
- [30] A. I. Titov, H. Takabe, B. Kämpfer, and A. Hosaka. "Enhanced subthreshold electron-positron production. in short laser pulses". *Phys. Rev. Lett.* **108**, 240406 (2012); A. I. Titov, B. Kämpfer, H. Takabe and A. Hosaka. "Breit-Wheeler process in very short electromagnetic pulses". *Phys. Rev. A* **87**, 042106 (2013).
- [31] A. I. Titov, B. Kämpfer, A. Hosaka, T. Nusch and D. Seipt. "Determination of the carrier envelope phase for short, circularly polarized laser pulses". *Phys. Rev. D* **93**, 045010 (2016).
- [32] A. Di Piazza. "Completeness and orthonormality of the Volkov states and the Volkov propagator in configuration space". *Phys. Rev. D* **97**, 056028 (2018).
- [33] A. Di Piazza. "Nonlinear Breit-Wheeler pair production in a tightly focused laser beam". *Phys. Rev. Lett.* **117**, 213201 (2016).
- [34] M. J. A. Jansen, J. Z. Kaminski, K. Krajewska, C. Müller. "Strong-field Breit-Wheeler pair production in short laser pulses: Relevance of spin effects". *Phys. Rev. D* **94** 013010, (2016).
- [35] M. J. A. Jansen, C. Müller. "Strong-Field Breit-Wheeler Pair Production in Short Laser Pulses: Identifying Multiphoton Interference and Carrier-Envelope-Phase Effects". *Phys. Rev. D* **93** 053011 (2016).
- [36] Zh. Wei, H. Han, W. Zhang, Y. Zhao, J. Zhu, H. Teng, and Q. Du. "Measurement and Control of Carrier-Envelope in Phase in Femtosecond Ti:sapphire Laser". In "Advances in Solid-State Lasers: Development and Applications". Book edited by: Mikhail Grishin, ISBN 978-953-7619-80-0, pp. 630, February 2010, INTECH, Croatia.
- [37] F. W. Helbing, G. Steinmeyer, and U. Keller. "Carrier-Envelope Control of Femtosecond Lasers with Attosecond Timing Jitter". *Laser Physics* **13**, 644 (2003).
- [38] T. Brabec and F. Krausz. "Intense few-cycle laser fields: Frontiers of nonlinear optics". *Rev. Mod. Phys.*, **72** 545 (2000).
- [39] J. X. Li, Y. Y. Chen, K. Z. Hatsagortsyan and C. H. Keitel, "Single-Shot Carrier-Envelope Phase Determination of Long Superintense Laser Pulses". *Phys. Rev. Lett.* **120**, 124803 (2018).
- [40] Y. F. Li *et al.*, "Determining the carrier-envelope phase of relativistic laser pulses via electron-momentum distribution". *Phys. Rev. A* **99**, 013850 (2019).
- [41] J. Li, R. Yu, P. Huang, A. Zheng, X. Yang. "Carrier-envelope phase-dependent electron tunneling in a coupled double-quantum-dot system driven by a few-cycle laser pulse". *Phys. Lett. A* **373**, 1896 (2009).
- [42] E. Cormier, P. Lambropoulos. "Effect of the initial phase of the field in ionization by ultrashort laser pulses". *Eur. Phys. J. D*, **2**, 15 (1998).
- [43] D. Seipt, D. Del Sorbo, C. P. Ridgers and A. G. R. Thomas. "Theory of radiative electron polarization in strong laser fields". *Phys. Rev. A* **98**, no. 2, 023417 (2018).
- [44] W. Greiner, J. Reinhardt. "Quantum Electrodynamics". Springer 2009, fourth edition.